Journal of Russian Laser Research, Volume 27, Number 4, 2006

NONLINEAR COHERENT DYNAMICS OF AN ATOM IN AN OPTICAL LATTICE

V. Yu. Argonov and S. V. Prants

Laboratory of Nonlinear Dynamical Systems, V. I. Il'ichev Pacific Oceanological Institute of the Russian Academy of Sciences, 43 Baltiiskaya Street, 690041 Vladivostok, Russia
e-mail: prants@poi.dvo.ru

Abstract

We consider a simple model of the lossless interaction between a two-level single atom and a standing-wave single-mode laser field which creates a one-dimensional optical lattice. The internal dynamics of the atom is governed by the laser field, which is treated as classical with a large number of photons. The center-of-mass classical atomic motion is governed by the optical potential and the internal atomic degrees of freedom. The resulting Hamilton–Schrödinger equations of motion are a five-dimensional nonlinear dynamical system with two integrals of motion, and the total atomic energy and the Bloch vector length are conserved during the interaction. In our previous papers, the motion of the atom has been shown to be regular or chaotic (in the sense of exponential sensitivity to small variations of the initial conditions and/or the system's control parameters) depending on the values of the control parameters, atom–field detuning, and recoil frequency. At the exact atom–field resonance, the exact solutions for both the external and internal atomic degrees of freedom can be derived. The center-of-mass motion does not depend in this case on the internal variables, whereas the Rabi oscillations of the atomic inversion is a frequency-modulated signal with the frequency defined by the atomic position in the optical lattice. We study analytically the correlations between the Rabi oscillations and the center-of-mass motion in two limiting cases of a regular motion out of the resonance: (1) far-detuned atoms and (2) rapidly moving atoms. This paper is concentrated on chaotic atomic motion that may be quantified strictly by positive values of the maximal Lyapunov exponent. It is shown that an atom, depending on the value of its total energy, can either oscillate chaotically in a well of the optical potential, or fly ballistically with weak chaotic oscillations of its momentum, or wander in the optical lattice, changing the direction of motion in a chaotic way. In the regime of chaotic wandering, the atomic motion is shown to have fractal properties. We find a useful tool to visualize complicated atomic motion – Poincaré mapping of atomic trajectories in an effective three-dimensional phase space onto planes of atomic internal variables and momentum. The Poincaré mappings are constructed using the translational invariance of the standing laser wave. We find common features with typical non-hyperbolic Hamiltonian systems – chains of resonant islands of different sizes imbedded in a stochastic sea, stochastic layers, bifurcations, and so on. The phenomenon of the atomic trajectories sticking to boundaries of regular islands, which should have a great influence on atomic transport in optical lattices, is found and demonstrated numerically.

Keywords: cold atoms, optical lattice, Hamiltonian chaos, fractals.

Manuscript submitted by the authors in English on July 1, 2006.

 1573-8760/06/2704-0360

1. Introduction

Light exerts mechanical forces on matter. This hypothesis was suggested by Kepler [1] in 1619 to explain the deviation of a comet's tail flying nearby the Sun. It was Maxwell who in 1873 estimated the light pressure, using his theory of electromagnetism [2], and who showed that it is very small. P. N. Lebedev was the first who in 1899 measured the light pressure on a macroscopic body [3]. The first experiments on deviation of microscopic particles by light were carried out by W. Gerlach and O. Stern [4], by P. Kapitza and P. Dirac [5], and by O. Frisch [6].

Manipulating by atomic motion with the help of laser beams, creating an optical lattice, is one of the most rapidly growing fields of modern physics (for a review, see, for example, [7]). There are different theoretical and experimental aspects of this interaction, including cooling and trapping of atoms, Bose–Einstein condensation, quantum computing, and processing information with atoms.

In this paper, we review our recent results on nonlinear coherent dynamics of a single two-level atom in an optical lattice created in a one-dimensional cavity by two counter-propagating laser waves. We are working in the strong-coupling regime and neglect all the losses. We show that, even in a one-dimensional approximation, the atomic motion can be very complicated. We analyze both regular and chaotic motion of atoms in a stationary standing-wave laser field containing a large number of photons. It should be stressed that there is a difference between various types of erratic atomic motion in an optical lattice. Chaotic motion is strictly defined as the motion of a deterministic nonlinear dynamic system that is exponentially sensitive to small variations in the system's initial conditions or/and its control parameters. There are different types of chaotic motion of atoms in an optical lattice, including chaotic nonlinear oscillations of the atomic center of mass in a well of the optical potential, chaotic ballistic motion where the atomic momentum oscillates chaotically around a value of the average momentum, and, last but not least, chaotic wandering of an atom when it changes its direction of motion in a chaotic way [8–13]. All types of chaotic atomic motion are quantified by positive values of the maximal Lyapunov exponent.

In an optical lattice, chaotic motion in the strict sense of this notation may occur when there is no noise of any kind, including atomic spontaneous emission, which is a random process. The respective deterministic atomic equations of motion are approximate ones, but they are fundamental since spontaneous emission may be considered as a quantum noise. *Random walking* is a kind of motion that occurs with ultracold atoms which are detuned far away from the carrier laser frequency, so their internal degrees of freedom can be eliminated adiabatically. Because the values of the momentum of ultracold atoms are compared with the value of the photon momentum, each time after emitting a spontaneous photon the atom gets a kick in a random direction. This effect is a quantum analog of the classical random walking.

In a generic situation, we should take into account both the internal atomic motion and spontaneous emission events. In this case, however, the equations of motion cease to be a deterministic dynamical system, because they include random terms, and one may expect much more complicated types of atomic motion which, besides chaotic motion caused by the fundamental atom-field interaction, includes a purely stochastic component caused by random events of spontaneous emission. We have shown recently that, in a range of the control parameters (detuning, laser intensity, and recoil frequency) and initial conditions, atoms may change their direction of motion erratically even if their momenta are much larger than the photon momentum. We will call this type of motion the chaotic walking.

The main aim of this paper is to describe different aspects of deterministic atomic motion in an optical lattice, both regular and chaotic ones. The effects of spontaneous emission on the atomic motion will be

considered in a forthcoming paper.

2. Hamilton–Schrödinger Equations of Motion

We consider a two-level atom with mass m_a and transition frequency ω_a, moving with momentum P along the X axis in an ideal cavity through the standing laser wave with field frequency ω_f and wave vector k_f. In a frame rotating with frequency ω_f, the standard cavity QED Hamiltonian reads

$$\hat{H} = \frac{\hat{P}^2}{2m_a} + \frac{1}{2}\hbar(\omega_a - \omega_f)\hat{\sigma}_z - \hbar\Omega\,(\hat{\sigma}_- + \hat{\sigma}_+)\cos k_f\hat{X}. \tag{1}$$

Here $\hat{\sigma}_{\pm,z}$ are the Pauli operators which describe the transitions between lower $|1\rangle$ and upper $|2\rangle$ states, and Ω is the Rabi frequency, which is proportional to the square root of the number of photons in the wave $\sqrt{n}$. The standing-wave field must be strong enough ($n \gg 1$) so that we can neglect the back reaction of atoms on the field and consider the field as a classical one. For the electronic degrees of freedom, the simple wave function is

$$|\Psi(t)\rangle = a(t)|2\rangle + b(t)|1\rangle, \tag{2}$$

where a and b are the complex-valued probability amplitudes of finding the atom in the states $|2\rangle$ and $|1\rangle$, respectively. Using the Hamiltonian (1), we get the Schrödinger equation

$$\begin{aligned} i\frac{da}{dt} &= \frac{\omega_a - \omega_f}{2}a - \Omega b\cos k_f X, \\ i\frac{db}{dt} &= \frac{\omega_f - \omega_a}{2}b - \Omega a\cos k_f X, \end{aligned} \tag{3}$$

where the atomic position X is considered as a parameter. Let us introduce instead of the complex-valued probability amplitudes a and b the following new real-valued variables:

$$u \equiv 2\,\mathrm{Re}\,(ab^*)\,, \qquad v \equiv -2\,\mathrm{Im}\,(ab^*)\,, \qquad z \equiv |a|^2 - |b|^2\,, \tag{4}$$

which are the quadratures of the atomic dipole moment (u and v) and the atomic population inversion z.

In the process of emitting and absorbing photons, atoms not only change their internal electronic states but their external translational states change as well due to the photon recoil. If the atomic average momentum is large in comparison with the photon momentum $\hbar k_f$, one can describe the translational degree of freedom classically as satisfying the classical Hamilton equations of motion. The dynamics in the strong-coupling regime is now governed by the Hamilton–Schrödinger equations

$$\begin{aligned} \dot{x} &= \omega_r p, \\ \dot{p} &= -u\sin x, \\ \dot{u} &= \Delta v, \\ \dot{v} &= -\Delta u + 2z\cos x, \\ \dot{z} &= -2v\cos x, \end{aligned} \tag{5}$$

where $x \equiv k_f\langle\hat{X}\rangle$ and $p \equiv \langle\hat{P}\rangle/\hbar k_f$ are the classical atomic center-of-mass position and momentum, respectively. The dot denotes differentiation with respect to the dimensionless time $\tau \equiv \Omega t$. The normalized recoil frequency $\omega_r \equiv \hbar k_f^2/m_a\Omega \ll 1$ and the atom–field detuning $\Delta \equiv (\omega_f - \omega_a)/\Omega$ are the control parameters. The system has two integrals of motion, namely, the total energy

$$W \equiv \frac{\omega_r}{2}p^2 + U, \tag{6}$$

where

$$U \equiv -u\cos x - \frac{\Delta}{2}z \tag{7}$$

is the potential energy, and the Bloch vector

$$u^2 + v^2 + z^2 = 1. \tag{8}$$

The conservation of the Bloch vector length immediately follows from Eqs. (4).

Equations (5) with two integrals of motion constitute a Hamiltonian autonomous system with two degrees of freedom and motion on a three-dimensional hypersurface with a given energy value W. Generally, such a system has a positive Lyapunov exponent λ, a negative exponent equal in magnitude to the positive one, and two zero exponents. The sum of all Lyapunov exponents of a Hamiltonian system is zero [14]. The maximal Lyapunov exponent characterizes the mean rate of exponential divergence of initially close trajectories

$$\lambda = \lim_{\tau\to\infty}\lambda(\tau), \qquad \lambda(\tau) = \lim_{\delta(0)\to 0}\frac{1}{\tau}\ln\frac{\delta(\tau)}{\delta(0)} \tag{9}$$

and serves as a quantitative measure of dynamical chaos in the system. Here, $\delta(\tau)$ is the distance (in the Euclidean sense) at time τ between two trajectories close to each other at the initial time $\tau = 0$. The dependence of λ on the control parameters has been calculated in [8,9] with a similar system. It has been shown that dynamical chaos in a strongly-coupled atom–field system exists in a wide range of parameters and initial atomic momentum p_0. The result of computation of the maximal Lyapunov exponent with our system (5) in the space of control parameters ω_r and Δ is shown in Fig. 1. In the white domains of the map, the maximal Lyapunov exponent λ is almost zero and the dynamics is stable. In the other domains, the positive values of λ show the Lyapunov instability.

In all the numerical simulations, we use physically realistic parameters and initial conditions. For example, we can choose cesium atoms with the transition wavelength $\lambda_a \simeq 852$ nm. The Rabi frequency Ω depends on many factors, including the field strength, which can be changed in a wide range. In most computations we use the Rabi frequency $\Omega \approx 10$ GHz. With this value of the Rabi frequency, we obtain the normalized recoil frequency to be $\omega_r = 10^{-5}$. Also we put the initial position $x_0 = 0$. The detuning Δ can be varied in a wide range, and the Bloch variables are restricted by the Bloch vector length (8). The most interesting effects are observed with rather cold atoms. For example, $p_0 = 200$ taken in computing λ in Fig. 1 with our normalization corresponds to the atomic velocity $v_a \approx 0.7$ m/s. It should be noted that in this paper we use normalization to the laser Rabi frequency Ω, not to the vacuum (or single-photon) Rabi frequency as has been done in our previous papers [8–12]. So the ranges of the normalized control parameters, taken in this paper, differ from those in the cited papers.

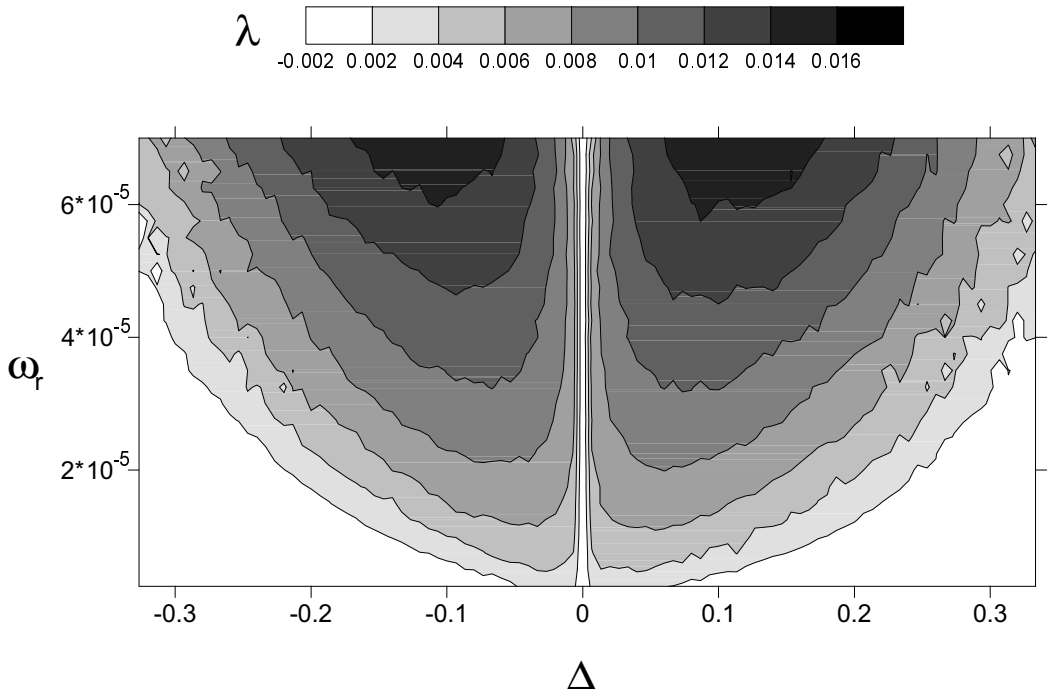

Fig. 1. Maximal Lyapunov exponent λ versus detuning Δ and normalized recoil frequency ω_r ($p_0 = 200$, $z_0 = -1$, and $u_0 = v_0 = 0$).

3. Regular Dynamical Regime

3.1. Exact Atom–Field Resonance

At the exact resonance $\Delta = 0$, one can easily find an additional integral of motion

$$u = \text{const.} = u_0. \tag{10}$$

In this case, the fast and slow variables are separated from each other, allowing one to integrate exactly the reduced equations of motion. The total energy becomes equal to

$$W_R = \frac{\omega_r}{2} p^2 - u_0 \cos x, \tag{11}$$

and the potential energy gets the simple form

$$U_R = -u_0 \cos x. \tag{12}$$

The center-of-mass translational motion of the atom in such a spatially periodic potential of the standing wave is described by the simple nonlinear equation for a free physical pendulum

$$\ddot{x} + \omega_r u_0 \sin x = 0 \tag{13}$$

and does not depend on evolution of the internal degrees of freedom.

The translational motion is trivial when u_0 is zero. In spite of the zero potential field, the structure of the standing wave is still present in the cavity. In this case, the atom will move in one direction with a constant velocity, and the Rabi oscillations modulated by the standing wave will occur. In the generic case, one can easily get from (11) the dependence $p(x)$

$$p = \sqrt{\frac{2}{\omega_r}(W_R + u_0 \cos x)}, \tag{14}$$

which gives the phase portrait of the system in the (x, p) plane (Fig. 2a). It is the phase portrait of a nonlinear pendulum with three types of trajectories depending on the value of its energy W_R: oscillator-like motion in a potential well if $W_R < u_0$, a separatrix if $W_R = u_0$, and ballistic-like motion if $W_R > u_0$.

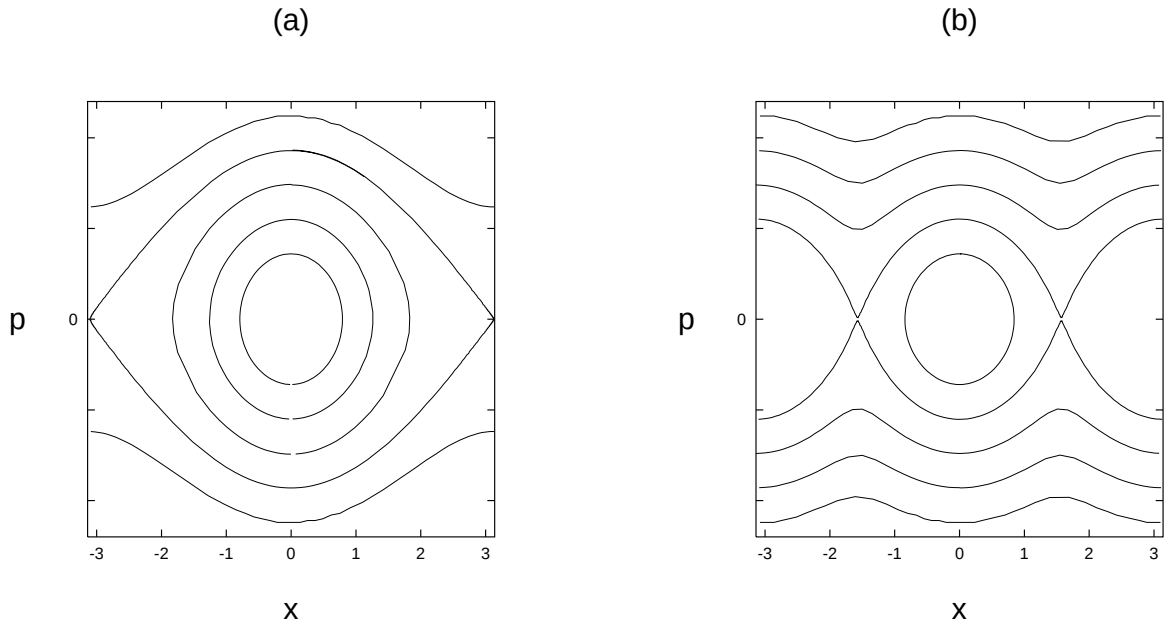

Fig. 2. Typical regular phase portraits of the translational degree of freedom with $\Delta = 0$ (a) and $|\Delta| \gtrsim 0.2$ (b).

For the initial values $x_0 = 0$ and $\dot{x}_0 = \omega_r p_0$, the equation for the translational motion (13) has the solution

$$x(\tau) = \begin{cases} 2 \arcsin\left(K \ \mathrm{sn}\left[\sqrt{\omega_r u_0}\tau, K\right]\right), & K^2 \leqslant 1, \\ 2 \ \mathrm{am}\left[\dfrac{1}{2}\omega_r p_0 \tau, \dfrac{1}{K}\right], & K^2 \geqslant 1, \end{cases} \tag{15}$$

$$p(\tau) = \begin{cases} p_0 \ \mathrm{cn}\left[\sqrt{\omega_r u_0}\tau, K\right], & K^2 \leqslant 1; \\ p_0 \ \mathrm{dn}\left[\dfrac{1}{2}\omega_r p_0 \tau, \dfrac{1}{K}\right], & K^2 \geqslant 1, \end{cases} \tag{16}$$

where

$$K = \frac{p_0}{2}\sqrt{\frac{\omega_r}{u_0}} \tag{17}$$

is the modulus of the elliptic Jacobi functions. The solution gives the critical value of the atomic momentum

$$p_{cr} = 2\sqrt{\frac{u_0}{\omega_r}}. \tag{18}$$

Atoms with $p_0 \leqslant p_{\rm cr}$ are trapped by the standing-wave field, a result that is well known from early studies [15]. The modulus K is simply connected with the normalized value of the difference between the atom energy and its value on the separatrix

$$K^2 = 1 + \frac{W_R - u_0}{2u_0}. \tag{19}$$

As to the internal atomic evolution, it depends on the translational degree of freedom since the force of the atom–field coupling depends on the atom position in a periodic standing-wave potential. The equation for the atomic population inversion $z(\tau)$ is derived from the two last equations of the set (5) with $\Delta = 0$

$$\dot{z} = \mp 2\sqrt{1 - z^2 - u_0^2}\cos[x(\tau)], \tag{20}$$

where $\cos[x(\tau)]$ is a known function of the translational variables which can only be found with the help of the exact solutions obtained. It is easy to find the exact solution of Eq. (20)

$$z(\tau) = \mp\sqrt{1 - u_0^2}\ \sin\left(2\int_0^\tau \cos x d\tau' + \psi_0\right), \tag{21}$$

where the sign is opposite to that for the initial value z_0 and

$$\psi_0 = \mp \arcsin\frac{z_0}{\sqrt{1 - u_0^2}} \tag{22}$$

is an integration constant. The internal energy of the atom can be considered as a frequency-modulated signal with the instant frequency $2\cos[x(\tau)]$ and the modulation frequency $\dot{x} = \omega_r p(\tau)$, but it is correct only if the first value is much greater than the second one, i.e., $|\omega_r p_0| \ll 2$. Such a signal is shown in Fig. 3a for a ballistic atom ($p_0 = 5000$, $v_a \approx 17.5$ m/s). With $|\omega_r p_0| \geqslant 2$, the modulation disappears and the signal becomes a periodic one with the frequency $\omega_r p$. With fast atoms $|\omega_r p_0| \gg 2$ and $p \simeq p_0 \gg p_{\rm cr}$ (Raman–Nath approximation) Eq. (21) is simplified:

$$z(\tau) \approx z_0 - \frac{2v_0}{\omega_r p_0}\sin\omega_r p_0\tau - \frac{4z_0}{\omega_r^2 p_0^2}\sin^2\omega_r p_0\tau. \tag{23}$$

3.2. Nonresonant Rabi Oscillations

With comparatively small detunings Δ, the dynamics of slow atoms can be chaotic. In this case, the Rabi oscillations are still a signal with a frequency modulation but the amplitude is not constant anymore; it jumps chaotically with the characteristic time $1/\omega_r p$. With comparatively large detunings, the Rabi oscillations become regular but with a prominent periodic amplitude modulation, while the frequency modulation is not so deep (Fig. 3b).

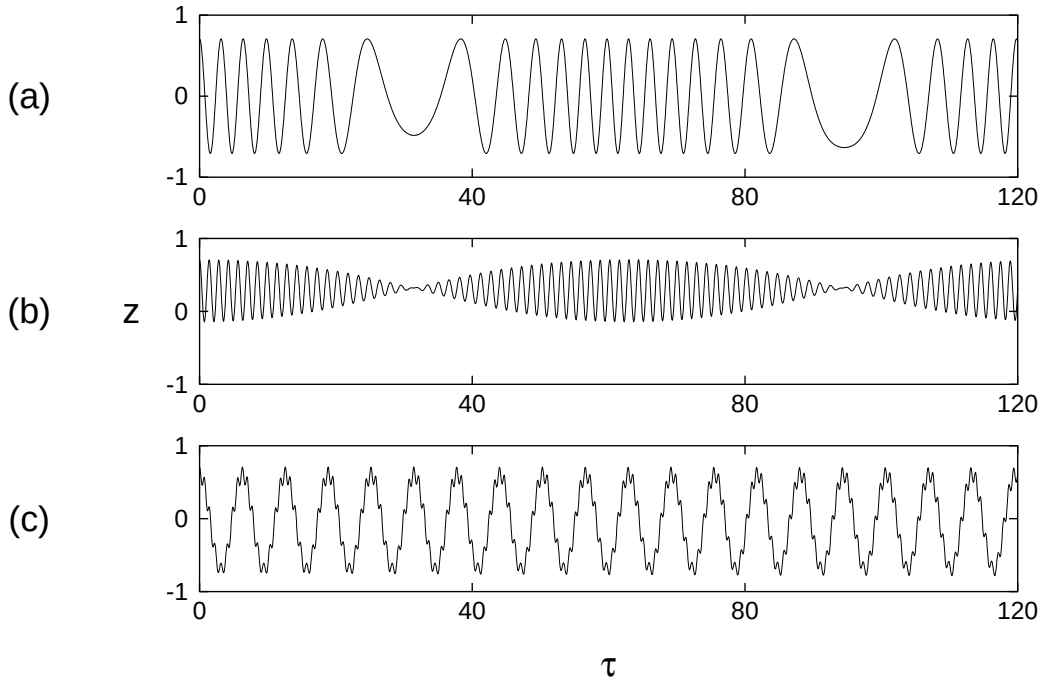

Fig. 3. Rabi oscillations: Frequency modulation at exact resonance $\Delta = 0$ and $p_0 = 5000$ (a), amplitude modulation far from resonance $\Delta = -4$ and $p_0 = 5000$ (b), and Doppler–Rabi resonance $\Delta = -4$ and $p_0 = 400000$ (c). In all panels, $z_0 = u_0 = \sqrt{0.5}$ and $v_0 = 0$.

In two limit cases $|\Delta| \gg \max[|\omega_r p|, 2]$ and $|\omega_r p| \gg \max[|\Delta|, 2]$, the analytic solutions can be obtained. In both cases, u and v are harmonic functions with frequency Δ, and for the internal energy we have

$$z \approx \begin{cases} z_0 + \dfrac{2u_0}{\Delta} - \dfrac{2\sqrt{u_0^2+v_0^2}}{\Delta}\cos x \sin(\Delta\tau + \varphi_0), & |\Delta| \gg \max[|\omega_r p|, 2], \\ z_0 + \dfrac{2\sqrt{u_0^2+v_0^2}}{\omega_r p_0}\cos(\Delta\tau + \varphi_0)\sin\omega_r p_0\tau, & |\omega_r p_0| \gg \max[|\Delta|, 2],\ \omega_r p_0^2 \gg 4, \end{cases} \tag{24}$$

where $\varphi_0 = \arcsin(u_0/\sqrt{u_0^2+v_0^2})$. The Rabi oscillations now are amplitude-modulated signals with two characteristic frequencies $|\omega_r p|$ and $|\Delta|$. The larger frequency is the main frequency and the other one is the modulation frequency. In the solution for fast atoms, we also used the Raman–Nath approximation $x \simeq \omega_r p_0 \tau$, which is correct if the initial kinetic energy $\omega_r p_0^2/2$ is much greater than the amplitude of potential energy variations (equal to 2 in our case). With $\Delta = 0$, the solution has the form (23) but without the last term, which is small. Solutions (24) show good correspondence with the numerical experiments performed in [12] with similar equations. The typical amplitude-modulated Rabi oscillations are shown in Fig. 3b.

The more exact solution for u can be found using the approximation $z \approx$ const. $\approx z_0$ (i.e., $z_{\max} - z_{\min} \ll |z_0|$), which is correct in both the limiting cases considered above, excluding $z_0 \approx 0$. Then from

Eq. (5) we get the equation for a driven linear oscillator

$$\ddot{u} + \Delta^2 u \approx 2z_0 \Delta \cos x, \tag{25}$$

which has the solution

$$\begin{aligned} u(\tau) \;\approx\; & 2z_0 \sin\Delta\tau \int \cos\Delta\tau \cos x d\tau - 2z_0 \cos\Delta\tau \int \sin\Delta\tau \cos x \, d\tau \\ & + u_0 \cos\Delta\tau + v_0 \sin\Delta\tau. \end{aligned} \tag{26}$$

For $|\Delta| \gg |\omega_r p|$, solution (26) can be approximated as follows:

$$u \approx \frac{2z_0}{\Delta} \cos x + \sqrt{u_0^2 + v_0^2}\ \sin(\Delta\tau + \varphi_0). \tag{27}$$

Using Eqs. (24) and (27), we get the periodic potential with the spatial period π (in contrast to the resonant potential with the period 2π)

$$U \approx -\frac{2z_0}{\Delta} \cos^2 x + \text{const}. \tag{28}$$

The corresponding phase portrait is shown in Fig. 2b.

When the frequencies are close $|\omega_r p| \simeq |\Delta|$, Doppler–Rabi resonance takes place [12] in spite of the fact that the detuning may be very large. Let us consider the standing wave as a combination of two counter-propagating waves. In the frame moving with the atomic velocity, their frequencies ω_1 and ω_2 are different because of the Doppler effect:

$$\omega_1 = \omega_f - \frac{v_a}{c}\omega_f, \qquad \omega_2 = \omega_f + \frac{v_a}{c}\omega_f, \tag{29}$$

where v_a is the atomic velocity and c is the velocity of light. The atom is rather slow, so we can neglect the relativistic effects. Let us consider atoms fast enough for the Raman–Nath approximation $p \approx p_0$ to be valid. Renormalizing all the frequencies to Ω, we define the dimensionless detunings between the atomic transition and the running wave frequencies as follows:

$$\Delta_1 \equiv \frac{\omega_1 - \omega_a}{\Omega} = \Delta - \omega_r p_0, \qquad \Delta_2 \equiv \frac{\omega_2 - \omega_a}{\Omega} = \Delta + \omega_r p_0. \tag{30}$$

The condition $|\Delta| = |\omega_r p_0|$ leads to the resonance between the atom and one of the waves. If $|\Delta| \gg 1$, we can neglect the interaction with the other wave and consider the atom as if only one wave with the frequency ω_1 or ω_2 exists. In the field of the wave, say ω_1, the dynamics can be described by the Bloch-like equations

$$\dot{u} = \Delta_1 v, \qquad \dot{v} = -\Delta_1 u + z, \qquad \dot{z} = -v, \tag{31}$$

in which the interaction energy does not depend on the atomic position and its amplitude value is two times smaller in comparison with the standing wave. Equations (31) have the solution

$$z = \frac{u_0 \Delta_1}{\omega_z^2}(1 - \cos\omega_z\tau) - \frac{v_0}{\omega_z} \sin\omega_z\tau + z_0 \left(\frac{\Delta_1^2}{\omega_z^2} + \frac{1}{\omega_z^2} \cos\omega_z\tau \right), \tag{32}$$

where $\omega_z \equiv \sqrt{\Delta_1^2 + 1} = \sqrt{(\Delta - \omega_r p_0)^2 + 1}$. At the exact Doppler resonance ($\Delta_1 = 0$), the atomic internal energy z oscillates with the dimensionless frequency 1, and the amplitude of oscillations is maximum. Numerical simulations with Eqs. (5) show that these speculations are correct (Fig. 3c, where $p_0 = 400000$ and $v_a \approx 1400$ m/s), and even very far from the resonance $\Delta = 0$ deep Rabi oscillations can be observed since the atoms are fast enough.

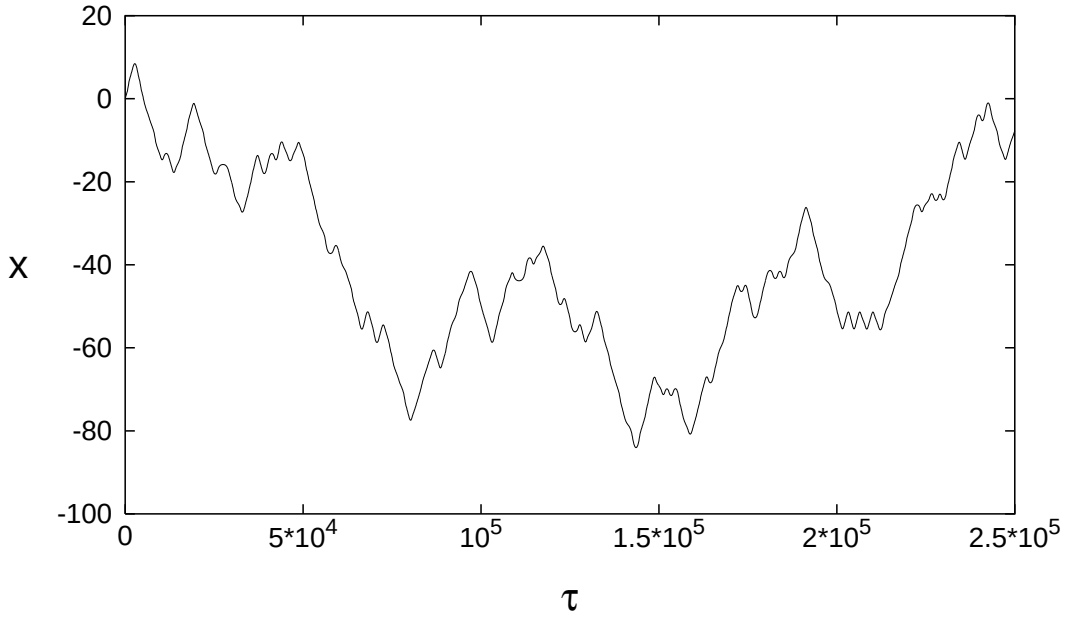

Fig. 4. Typical atomic trajectory in the regime of chaotic wandering ($x_0 = 0$, $p_0 = 300$, $z_0 = -1$, $u_0 = v_0 = 0$, $\omega_r = 10^{-5}$, and $\Delta = -0.05$).

4. Irregular Dynamics: Chaos and Fractals

4.1. Chaotic Atomic Wandering

In Fig. 1 we depict the maximal Lyapunov exponent map in the space of control parameters ω_r and Δ. The maximal Lyapunov exponent depends not only on the parameters ω_r and Δ but on the initial conditions of the system of equations (5) as well. Especially important is the value of the initial momentum p_0. The most interesting effects can be observed with rather cold atoms, when the initial atomic kinetic energy is close to the amplitude of the optical potential. In this case, we get the chaotic wandering of an atom in a standing wave. A typical chaotic atomic trajectory is shown in Fig. 4.

It follows from (5) that the translational motion of the atom at $\Delta \neq 0$ is described by the equation of a nonlinear physical pendulum with a frequency modulation

$$\ddot{x} + \omega_r u(\tau) \sin x = 0, \tag{33}$$

in which u is the function of all the other dynamical variables. The normalized Rabi oscillation frequency is of the order of $\omega_z' \equiv \sqrt{\Delta^2 + 4}$, which substantially exceeds the frequency of small-amplitude translational motion $\sqrt{\omega_r u_0} \ll 1$ in the potential well. Taking this into consideration, the mechanism of the arising chaos can be revealed [10]. The stochastic layer width was estimated to be

$$D \simeq 8\pi \left(\frac{\omega_z'}{\omega_0}\right)^3 \exp\left(\frac{-\pi\omega_z'}{2\omega_0}\right), \tag{34}$$

where $\omega_0 \equiv \sqrt{2\omega_r|\Delta|}/\omega_z'$ and $\omega_z'/\omega_0 \gg 1$. The D value is the energy change in the neighborhood of the unperturbed separatrix normalized with respect to the pendulum separatrix energy ω_0^2. Small changes

in the energy causes comparatively small changes in the frequency of oscillations. For energies of motion that are strongly different from the separatrix energy, that is, close to the potential well bottoms and high above the optical potential U hills, small frequency changes cause small phase changes during the translation-motion period. However, close to the unperturbed separatrix, where the period of oscillations tends to infinity, even small frequency changes can cause substantial phase changes. This is the reason for the exponential instability of motion of the parametric nonlinear oscillator (33) and chaotic atomic motion in the field of a periodic standing wave.

A clear idea of the character of chaotic wandering can be developed using the model of "two potentials." At resonance, the optical potential U reproduces the structure of the standing wave in the cavity (12) with the period 2π (the phase portrait in Fig. 2a). Far from resonance, the potential has the period π and is approximately described by Eq. (28), and the corresponding phase portrait is shown in Fig. 2b. These potentials will be called resonant and nonresonant, respectively. We can say that when the motion in the cavity is chaotic, both potentials "virtually" coexist. The well depths in both structures change as time passes, and an atom randomly gets into one or another structure every time it crosses a standing-wave node. The probability of getting into the resonant or nonresonant potentials depends on the detuning. Near resonance the atom is in the resonant potential almost the whole time and only rarely gets into the nonresonant one for a short time.

In our study [12] we have shown that chaotic wandering has fractal properties.

4.2. Dynamical Atomic Fractals

In Fig. 5 we depict the scheme of a gedanken experiment that consists of a Fabry–Perot optical microcavity with two detectors and cold atoms placed in the cavity. To avoid complications that are

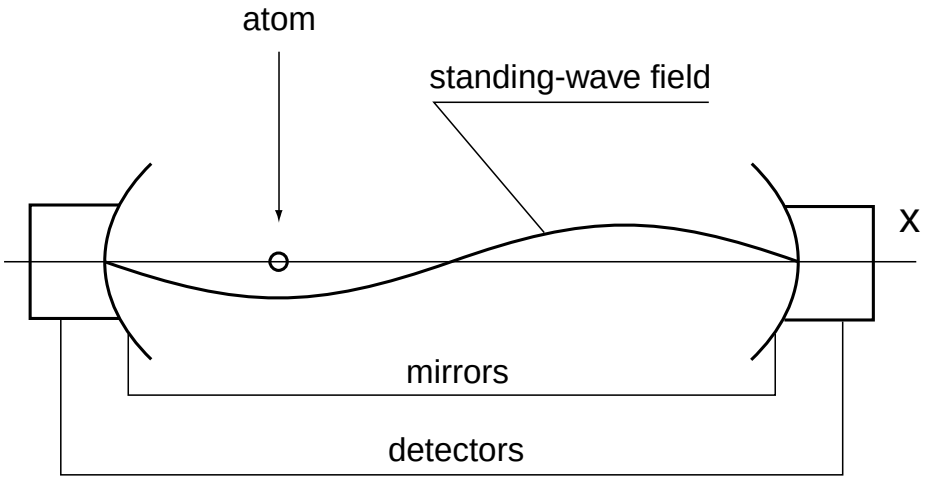

Fig. 5. Schematic diagram of a standing-wave microcavity with detectors.

not essential to the main theme of this work, we consider a cavity with only two standing-wave lengths. Atoms, one by one, are placed at the point $x_0 = 0$ with different values of the detuning Δ. We measure time T at which an atom reaches one of the detectors (exit time) and study the dependence $T(\Delta)$ under

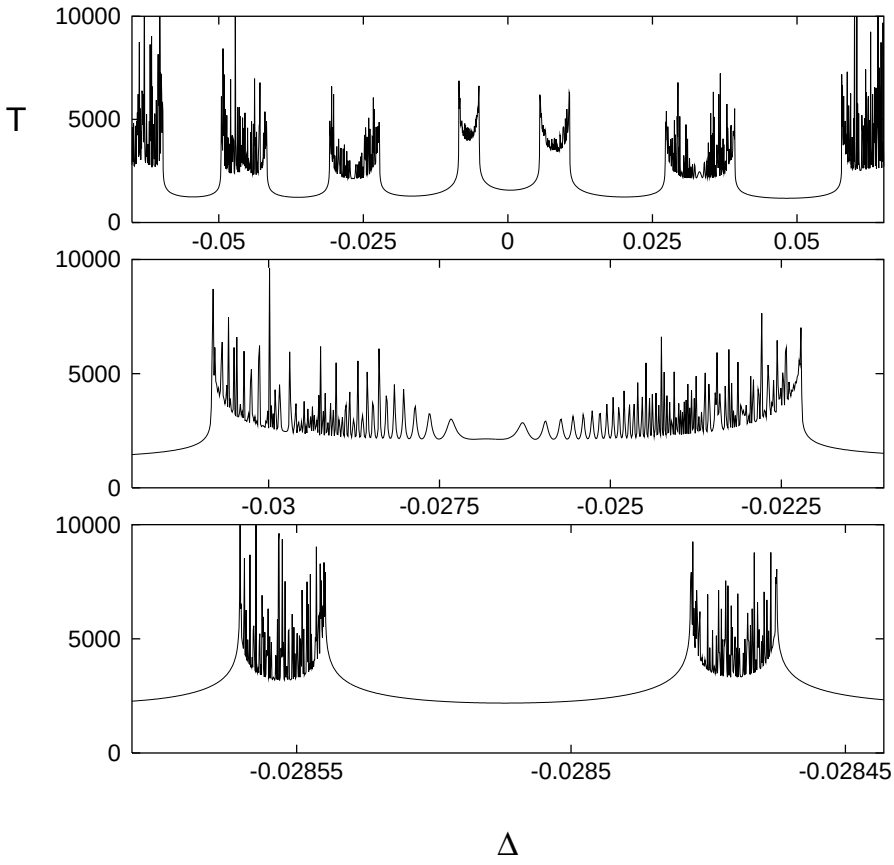

Fig. 6. Atomic fractals. Exit time of cold atoms T vs the detuning Δ: $p_0 = 200$, $z_0 = -1$, $u_0 = v_0 = 0$.

other equal conditions imposed on the atom and the cavity field. Figure 6 shows the function $T(\Delta)$ for atoms with the initial momentum $p_0 = 200$ ($v_a \approx 0.7$ m/s). The exit time function demonstrates the intermittency of the smooth curves and the complicated structures, which cannot be resolved in principle no matter how large the magnification factor. The middle and low panels in Fig. 6 show successive magnifications of the function for small intervals. Further magnifications reveals a self-similar fractal-like structure that is typical for Hamiltonian systems with chaotic scattering [16].

The exit time T corresponding to both smooth and unresolved Δ intervals increases with increase in the magnification factor. Theoretically, there exist atoms never reaching the detectors in spite of the fact that they have no obvious energy restrictions to leave the cavity. The tiny interplay between chaotic external and internal dynamics prevents these atoms from leaving the cavity. A similar phenomenon in chaotic scattering is known as dynamical trapping. In [12] for a similar fractal we have computed the Hausdorff dimension and shown that it is not integer.

The different kinds of atomic trajectories before the detection can be characterized by the number $m - 1$ of sign changes of the momentum. An mth trajectory corresponds to an atom which changes the direction of motion before being detected $m - 1$ times. There are also special separatrix-like trajectories

following which atoms asymptotically approach the points with the maximum of potential energy, having no more kinetic energy to overcome it. In contrast to the separatrix motion in the resonant system ($\Delta = 0$) with the initial atomic momentum $p_{\rm cr}$, a detuned atom can asymptotically reach one of the stationary points even after several oscillations in a well. Let us define the mS-trajectory as a trajectory where the atom changes the direction of motion $m-1$ times and then the separatrix-like motion begins. Such asymptotic motion takes infinite time, the atom will never be detected.

The smooth Δ intervals in the first-order structure (Fig. 6, upper panel) correspond to atoms which never change the direction of motion, i.e., $m = 1$, and reach the right detector. The unresolved singular points in the first-order structure with $T = \infty$ at the border between the smooth and unresolved Δ intervals are generated by the $1S$-trajectories. Analogously, the smooth and unresolved Δ intervals in the second-order structure (Fig. 6, middle panel) correspond to the second-order and other trajectories, respectively, with singular points between them corresponding to the $2S$-trajectories, and so on.

There are two different mechanisms of generation of infinite detection times, namely, dynamical trapping with infinite oscillations ($m = \infty$) in a cavity and the separatrix-like motion ($m \neq \infty$). The set of all detunings generating the separatrix-like trajectories is a countable fractal. Each point in the set can be specified as a vector in a Hilbert space with m integer nonzero components. One is able to prescribe to any unresolved interval of mth order structure a set with m integers, where the first integer is a number of a second-order structure to which the trajectory under consideration belongs in the first-order structure, the second integer is a number of a third-order structure in the second-order structure mentioned above, and so on. Such a number set is analogous to a directory tree address: "<a subdirectory of the root directory>/<a subdirectory of the 2nd level>/<a subdirectory of the 3rd level>/... Unlike the separatrix fractal, the set of all detunings leading to dynamically trapped atoms with $m = \infty$ seems to be uncountable.

The scattering function in the regime of chaotic wandering (time of exit T) depends in a complicated way not only on the control parameters but on the initial conditions as well. In Fig. 7 we demonstrate the view of this function, whose values are modulated by grey scale darkness in two coordinates — the initial atomic momentum p_0 and the atom–field detuning Δ. From the fragment (a) to the fragment (f), we increase subsequently the resolution. One can see the increasing complexity of the scattering function with a prominent self-similarity. The computation has been performed with the recoil frequency $\omega_r = 9.17 \cdot 10^{-5}$.

4.3. Poincaré Mapping

The five variables in the equations of motion (5) minus the two integrals of motion (6) and (8) provide the motion in a three-dimensional space. To visualize the motion, we use the idea of mapping trajectories on two-dimensional planes. Since we have no time-periodic perturbations in our equations of motion (5), we cannot map trajectories through equal intervals of time provided by the period of a perturbation. However, the system has a characteristic space period 2π imposed by the standing wave. So we map the trajectories on a chosen plane at those time moments when the atoms reach the positions where $\cos x = 1$. We close our phase space along the position variable with the period 2π. The condition $\cos x = 1$ under fixed values of the integrals of motion (6) and (8) defines a closed two-dimensional surface the phase-space points of which characterize unambiguously the system's states. In other words, there is a set of points on this two-dimensional surface which corresponds to each trajectory with a given value of the energy W. This set can be projected onto a plane of any system's variables except for the position x. Such

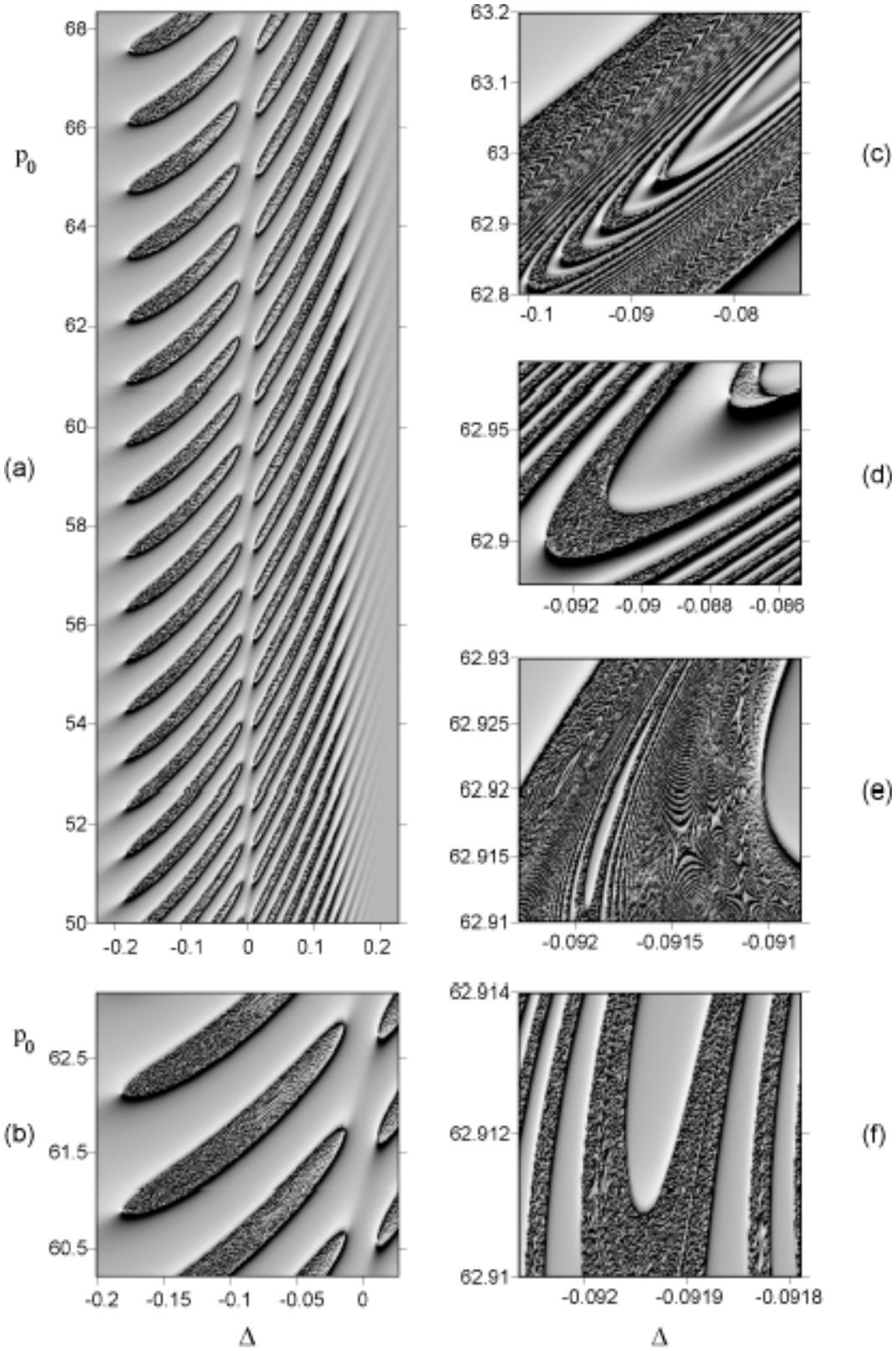

Fig. 7. Fractal function of the exit time T versus the detuning Δ and the initial momentum p_0. The function is shown in a shaded relief regime with $\omega_r = 9.17 \cdot 10^5$.

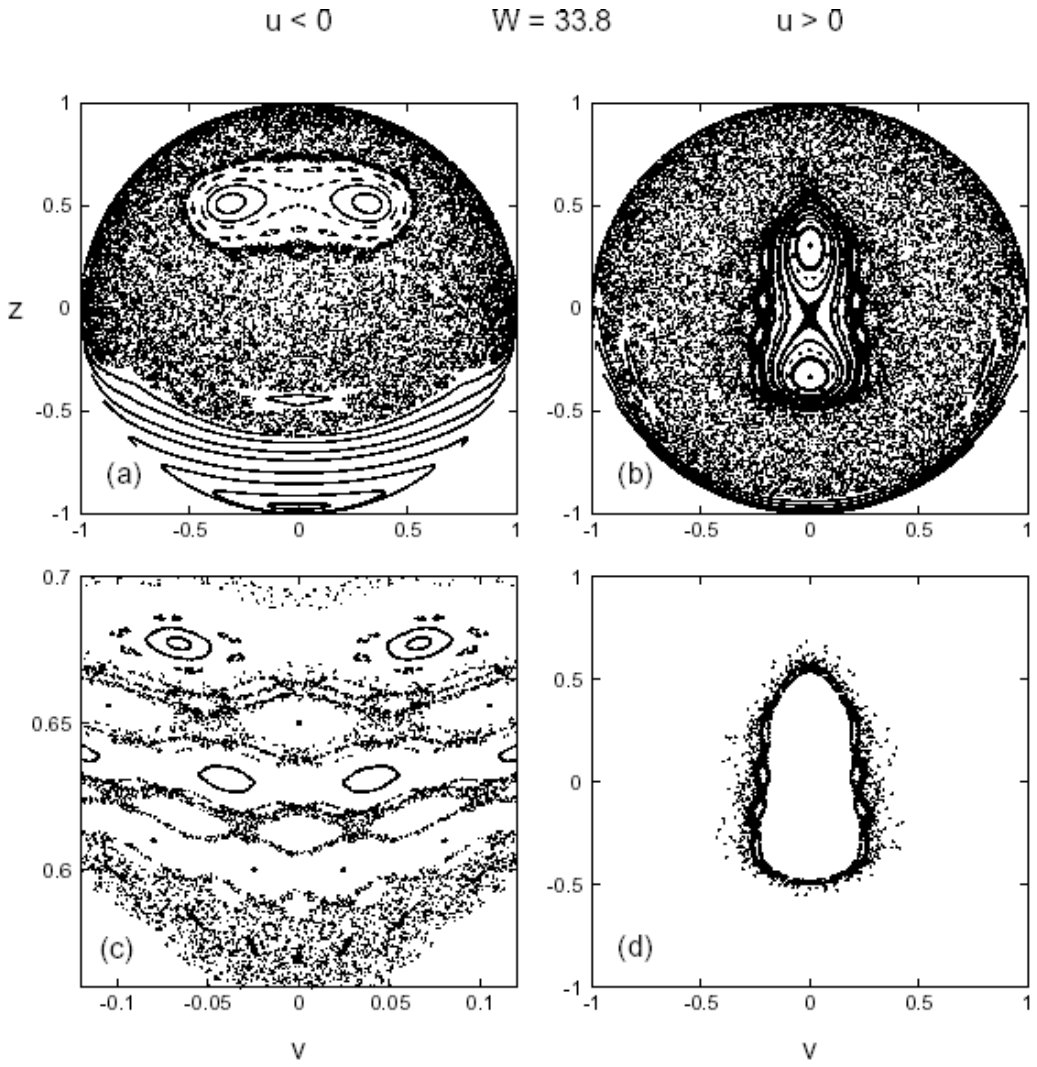

Fig. 8. Poincaré mapping in the Bloch variable space: $u < 0$, western Bloch hemisphere (a), $u > 0$, eastern Bloch hemisphere (b), magnification of the small region in (a) fragment (c), and mapping with a single chaotic trajectory in (b) fragment, illustrating the effect of sticking (d) at $W = 33.8$, $p_{\text{eff}} = 2600$, $\omega_r = 10^{-5}$, and $\Delta = -0.05$.

a projection is, generally speaking, two-valued because the two-dimensional surface is closed. However, one can map trajectories in its "eastern" and "western" parts separately.

In Fig. 8a and b, we demonstrate the Poincaré mappings of a number of atomic trajectories in the western ($u < 0$) and eastern ($u > 0$) hemispheres of the Bloch sphere (u, v, z) on the $v - z$ plane, respectively. We fix the values of the detuning $\Delta = -0.05$, the recoil frequency $\omega_r = 10^{-5}$, the total energy $W = 33.8$, and the initial position $x_0 = 0$ and map the trajectories with other different initial conditions, which are restricted by (6) and (8). All the mappings were obtained with ballistic atoms whose momenta slightly (but chaotically for some initial conditions) oscillate around the effective value $p_{\text{eff}} = 2600$, which corresponds to the chosen energy value. This is the value of the momentum that an

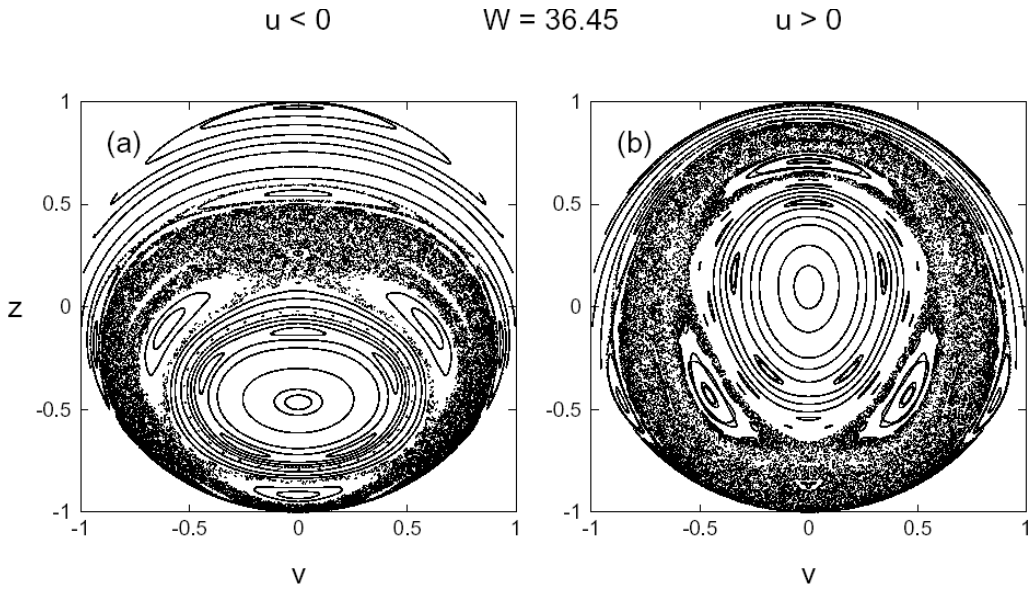

Fig. 9. Poincaré mapping in the Bloch variable space: $u < 0$, western Bloch hemisphere (a) and $u > 0$, eastern Bloch hemisphere (b). The parameters are the same as in Fig. 8 but $W = 36.45$ and $p_{\text{eff}} = 2700$.

atom has at the moments when its potential energy U is zero. In Fig. 9 we demonstrate the Poincaré mappings of a number of atomic trajectories in the western ($u < 0$) and eastern ($u > 0$) hemispheres of the Bloch sphere (u, v, z) on the $v - z$ plane just as in Fig. 8 with $W = 33.8$ but with the other value of the total energy $W = 36.45$ and the effective momentum $p_{\text{eff}} = 2700$. A series of bifurcations occurs just between these values of energy and we get in the end a central critical point instead of a saddle. One can see a typical structure with surviving nonlinear resonances of different orders around the center point and overlapping resonances.

In Figs. 8a, 8b, and 9, general views of the mappings in the western and eastern hemispheres are shown. The pictures are rather typical with chaotic Hamiltonian systems [17]. We see regions of regular motion in the form of islands and chains of islands filled by regular trajectories which are known as Kolmogorov–Arnold–Moser (KAM) invariant curves. The islands are imbedded into a stochastic sea, and they are produced by nonlinear resonances of different orders. Increasing the resolution of the mapping, one can see that big islands are surrounded by islands of smaller size each of which, in turn, is surrounded by a chain of even smaller islands, and so on to infinity. Stochastic layers of the ∞-like form are situated between the islands. From the physical point of view, they are formed by broken and overlapping nonlinear resonances. From the mathematical point of view, a stochastic layer is a heteroclinic structure formed by transversal intersections of stable and unstable manifolds of hyperbolic stationary points. A fractal-like structure of generations of islands, a trademark of Hamiltonian chaos, is clearly seen on projections of the motion in both the western and eastern hemispheres. To illustrate what happens upon increasing the resolution of the Poincaré mapping, we plot in Fig. 8c a close-up of a small region in the stochastic layer in Fig. 8a.

We would like to pay attention to another typical phenomena in Hamiltonian systems, the so-called sticking [17–21]. In Fig. 8d we demonstrate the phenomenon of sticking in the eastern Bloch hemisphere.

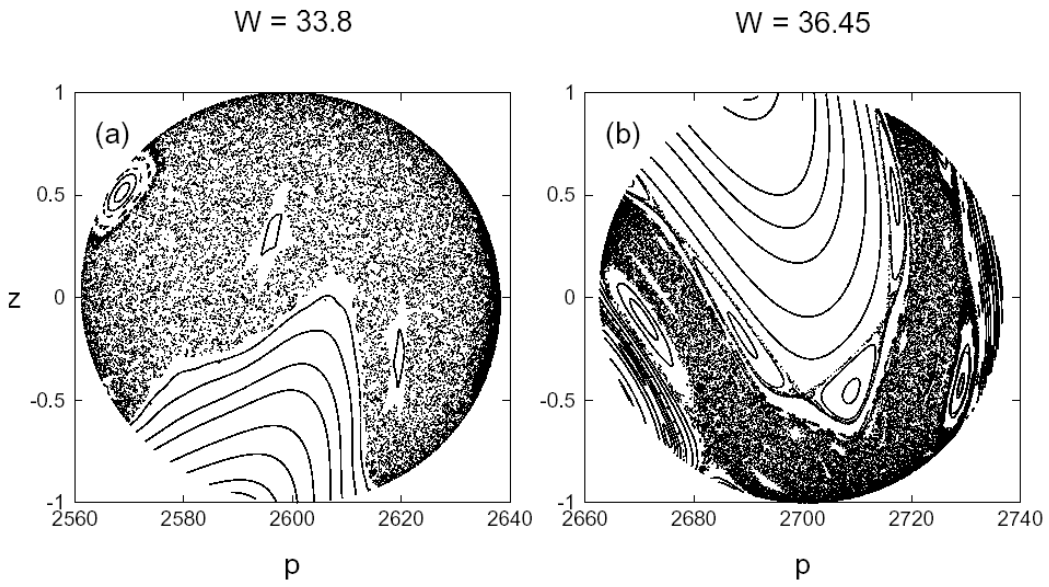

Fig. 10. Poincaré mapping in the space of the momentum p and the internal energy z: $W = 33.8$ and $p_{\text{eff}} = 2600$ (a) and $W = 36.45$ and $p_{\text{eff}} = 2700$ (b). The other parameters are the same as in Fig. 8.

The trajectory shown demonstrates an intermittent type of motion. It wanders for a while in the stochastic sea as a chaotic trajectory, whose instability is characterized by a positive value of the finite-time maximal Lyapunov exponent. Then it is stuck to the boundaries of the outermost visible chain of regular islands, where it is practically regular with a zero value of the respective finite-time maximal Lyapunov exponent. It may take a large amount of time to find a gap in a cantori structure, surrounding the outermost KAM tori, and to get off in the stochastic sea. The process is repeated as time grows. It should be stressed that sticking influences strongly transport properties in Hamiltonian systems, giving rise to anomalous diffusion, and algebraic tails in the distributions of the Poincaré recurrence times and of times and lengths of atomic flights.

In Fig. 10, we map the same atomic trajectories as in Figs. 8 and 9 onto the $p - z$ plane. In this case, both parts of the closed two-dimensional surface have the same projections because the set is symmetric with respect to the hyperplane $v = 0$.

In order to quantify the instability of the trajectories on the Poincaré mappings in Figs. 8 and 9, we have computed the maps of the maximal Lyapunov exponents exactly with the same initial conditions and parameters as in those figures. The results in $v_0 - z_0$ coordinates for eastern hemispheres at $W = 33.8$ and $W = 36.45$ with $u > 0$ are shown in Figs. 11a and 11b, respectively. The rather good correspondence between the Poincaré mapping and the maximal Lyapunov exponents proves that the Poincaré mapping we have constructed is a good means to visualize the complicated dynamics of coupled internal and external atomic degrees of freedom.

A Poincaré mapping with a rich structure of regular and chaotic domains is typical only in a range of values of the total energy W. At values $W \gtrsim 40$, the atoms move regularly and the respective Poincaré mapping consists of regular invariant curves only. With decreasing the energy, a series of bifurcations occurs with the appearance of resonant islands of different order. Upon decreasing the energy even more,

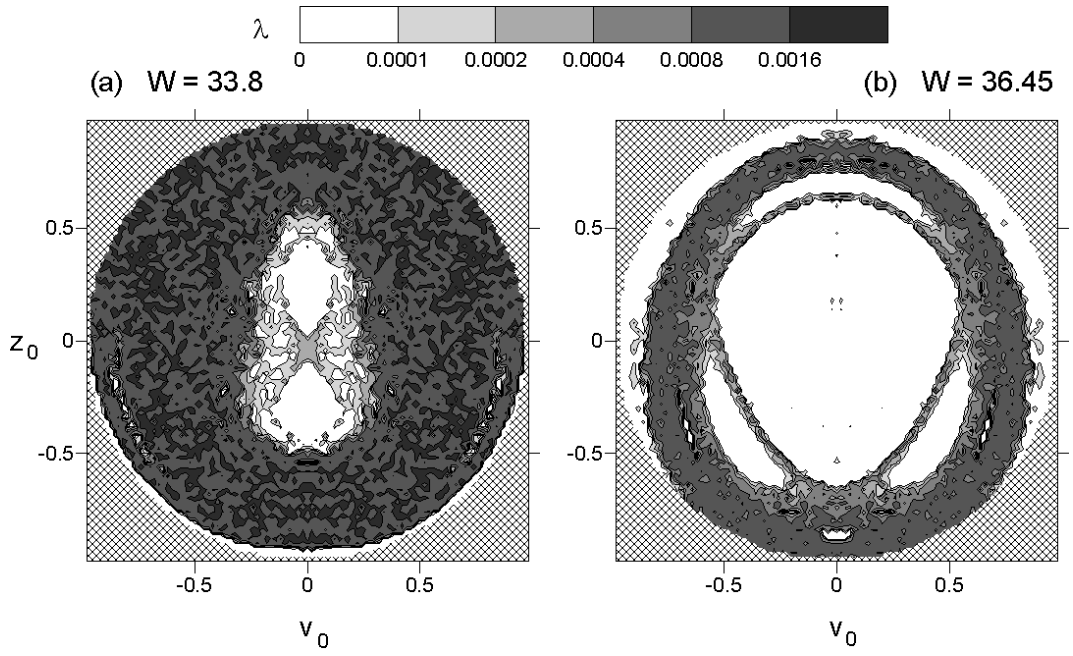

Fig. 11. Maximal Lyapunov exponent versus the initial values of the Bloch variables v_0 and z_0 with $u_0 > 0$: $W = 33.8$ and $p_{\text{eff}} = 2600$ (a) and $W = 36.45$ and $p_{\text{eff}} = 2700$ (b). The other parameters are the same as in Fig. 8.

global chaoticity takes place. At the exact resonance $\Delta = 0$, the value $W = u_0$ corresponds to a separatrix in mechanical variables. Out of the resonance, this separatrix is broken and the atoms may wander chaotically in the optical lattice with the respective irregular Poincaré mapping. At $W \lesssim u_0 + \Delta z_0/2$ (including negative values), the atoms are trapped in wells of the optical potential and oscillate there.

5. Conclusions

We have considered a simple model of the lossless interaction between a two-level single atom and a standing-wave single-mode laser field which creates a one-dimensional optical lattice. Analytical solutions of the Hamilton–Schrödinger equations of motion have been derived and analyzed in some limiting cases of regular atomic motion. Correlations between the Rabi oscillations and the center-of-mass motion have been established and demonstrated. In the regime of chaotic wandering, the atomic motion has been shown to have fractal properties. Using a special type of Poincaré mapping of atomic trajectories in an effective three-dimensional phase space onto planes of atomic internal variables and momentum, we have found typical structures in Hamiltonian chaotic systems – chains of resonant islands of different sizes imbedded in a stochastic sea, stochastic layers, bifurcations, and so on. The phenomenon of sticking of atomic trajectories to the boundaries of regular islands found in numerical experiments should have a great influence on atomic transport in optical lattices.

One of the aims of this paper was to describe analytically and numerically the fundamental aspects of nonlinear dynamics of atom–field interaction. We have done that to some extent at the cost of simplifying the model. To be more realistic, we should take into account spontaneous emission events. In this case,

however, the equations of motion cease to be a deterministic dynamical system because they would include random terms. Our previous results on Monte Carlo modeling of Hamilton–Schrödinger equations have shown much more complicated types of atomic motion which, besides chaotic motion caused by the fundamental atom–field interaction, include a purely stochastic component caused by random events of spontaneous emission. We plan to study the effects of spontaneous emission on chaotic atomic motion in the future.

Acknowledgments

This work was supported by the Russian Foundation for Basic Research under Project No. 06-02-16421 "Quantum nonlinear dynamics of cold atoms in an optical lattice", by the Program "Mathematical methods in nonlinear dynamics" of the Presidium of the Russian Academy of Sciences under the Project "Dynamical chaos and coherent structures," and by the Program of the Presidium of the Far-Eastern Division of the Russian Academy of Sciences under Projects "Nonlinear quantum electrodynamics of atoms and photons" and "Dissipative dynamics of cold atoms in optical lattices."

References

1. J. Kepler, *The Harmonies of the World*, Encyclopedia Britannica, Chicago (1952).
2. J. C. Maxwell, *A Treatise on Electricity and Magnetism*, Dover, New York (1954).
3. P. N. Lebedev, *Collected Papers* [in Russian], GITTL, Moscow-Leningrad (1949).
4. W. Gerlach and O. Stern, *Z. Phys.*, **9**, 349 (1922).
5. P. L. Kapitsa and P. A. M. Dirac, *Proc. Cambridge Philos. Soc.*, **29**, 297 (1933).
6. O. Frisch, *Z. Phys.*, **86**, 42 (1933).
7. S. Chu, *Rev. Mod. Phys.*, **70**, 685 (1998); C. Cohen-Tannoudji, *Rev. Mod. Phys.*, **70**, 707 (1998); W. D. Phillips, *Rev. Mod. Phys.*, **70**, 721 (1998).
8. S. V. Prants and L. E. Kon'kov, *JETP Lett.*, **73**, 180 (2001) [*Pis'ma ZhÉTF*, **73**, 200 (2001)].
9. S. V. Prants and V. Yu. Sirotkin, *Phys. Rev.* A, **64**, 033412 (2001).
10. S. V. Prants, *JETP Lett.*, **75**, 63 (2002) [*Pis'ma ZhÉTF*, **75**, 71 (2002)].
11. S. V. Prants, *JETP Lett.*, **75**, 651 (2002) [*Pis'ma ZhÉTF*, **75**, 777 (2002)].
12. V. Yu. Argonov and S. V. Prants, *JETP*, **96**, 832 (2003) [*Zh. Éksp. Teor. Fiz.*, **123**, 946 (2003)].
13. S. V. Prants, M. Edelman, and G. M. Zaslavsky, *Phys. Rev.* E, **66**, 046222 (2002).
14. A. J. Lichtenberg and M. A. Lieberman, *Regular and Stochastic Motion*, Springer, New York (1983).
15. V. S. Letokhov, *JETP Lett.*, **7**, 348 (1968) [*Pis'ma ZhÉTF*, **7**, 348 (1968)].
16. E. Ott, *Chaos in Dynamical Systems*, Cambridge University Press, Cambridge (1993).
17. G. M. Zaslavsky, *Hamiltonian Chaos and Fractional Dynamics*, Oxford University Press, Oxford (2005).
18. C. F. F. Karney, *Physica* D, **8**, 360 (1983).
19. B. V. Chirikov and D. L. Shepelyansky, *Physica* D, **13**, 394 (1984).
20. J. D. Meiss, *Rev. Mod. Phys.*, **64**, 795 (1992).
21. V. V. Beloshapkin and G. M. Zaslavsky, *Phys. Lett.* A, **97**, 121 (1993).